Gasdynamic Measurements
LASL Intense Neutron Sou

S. C. Johnston

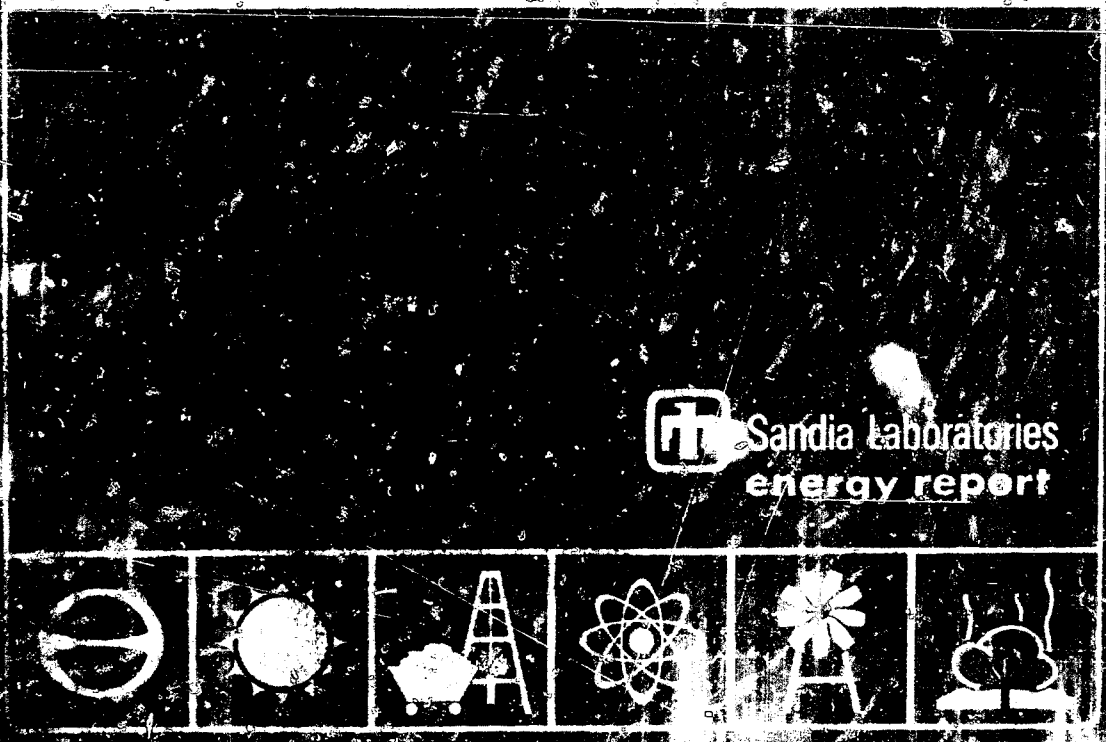

SAND 2909-0

SAND77-8294
Unlimited Release
Printed February 1978

GASDYNAMIC MEASUREMENTS FOR THE LASL INTENSE NEUTRON SOURCE

S. C. Johnston
Combustion Applications Division 8352
Sandia Laboratories, Livermore, California

ABSTRACT

Measurements made on a two-dimensional simulation of the Los Alamos Scientific Laboratory (LASL) Intense Neutron Source (INS) experiment are discussed. The purpose of this work was to characterize the supersonic INS channel flow under conditions of large amounts of energy deposition. Nozzle channel wall pressure measurements, cold flow leakage rates, vacuum channel pressure and Mach number, leakage flow rates with mass addition to and momentum extraction from the main flow, and flow visualization photographs are given. Energy addition up to thirty percent of the theoretical maximum was achieved via mass addition to and momentum extraction from the main channel flow. In this range, both a weak and strong shock regime for leakage flow were identified. These regimes differed by about twenty percent in leakage flow rates.

ACKNOWLEDGMENTS

The author wishes to thank Ken Hencken and Jim Gruver for their extensive contributions to this experiment.

GASDYNAMIC MEASUREMENTS FOR THE LASL INTENSE NEUTRON SOURCE

Introduction

This document is the final report on the experimental gasdynamic research done through August, 1977 by Sandia Laboratories, Livermore for the Department of Energy's Division of Magnetic Fusion Energy. The work was done in support of the Intense Neutron Source (INS) project at the Los Alamos Scientific Laboratory (LASL). Since the INS research at LASL (and with it the support work at Sandia) has been cancelled, the results reported here are incomplete.

The purpose of the LASL project was to build a neutron source that would accurately simulate a fusion reactor environment to test and develop materials to be used for containment of the fusion reaction. In the LASL design, a coaxial supersonic flow of deuterium (Figure 1) would provide both the gas target for a 270 keV, 1.1 amp tritium ion beam and the means of dissipating the 1/3 megawatt of heat deposited in the D-T interaction zone. The resulting D-T reaction at the target (which was to be about 1 cm^3 in volume) was hoped to produce a continuous neutron flux of 10^{15} neutrons/sec. This neutron flux was designed to irradiate the walls of the expansion nozzle, which was to be constructed of the material under test.

From a gasdynamic viewpoint, the phenomena considered to be important in the INS design included: (1) the possibility of a significant leakage flow of deuterium back up the tritium ion beam port, which for purposes of ion beam transport had to be kept at a pressure of about 1 torr; and (2) choking of the supersonic deuterium flow due to heat addition causing increased static pressures in the D-T interaction region (and thus more flow up the ion beam port) and an inability of the deuterium flow to dissipate the heat deposited in the interaction zone.

Sandia's experiment (Figure 2) was to simulate the energy deposition region in the INS using chemical energy deposition. In this experiment, combustible gases were introduced into the main flow via an opposed jet. Jet momentum was dissipated by the main flow some distance downstream of the combustible gas nozzle exit. This caused the opposed-jet to turn back on itself and flow with the main stream. Ignition of the combustible gases was to have provided the required energy deposition. In contrast to the INS axisymmetric design, the Sandia experiment was two-dimensional, having glass windows for optical access to the entire flow.

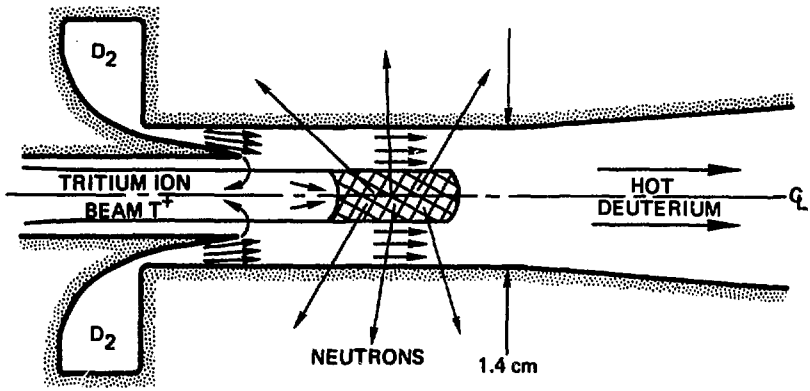

Figure 1. LASL Intense Neutron Source (INS)

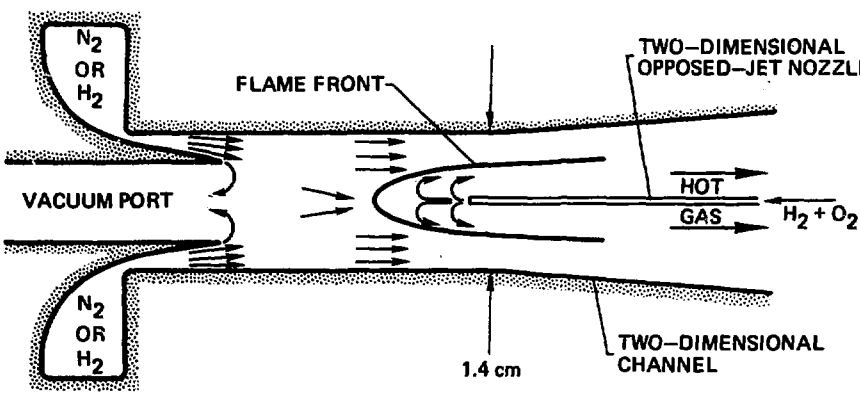

Figure 2. INS Simulation Experiment-Chemical Energy Deposition

EXPERIMENTAL APPARATUS

The experimental apparatus consisted of a two-dimensional flow channel fed by two identical supersonic nozzles (Figure 3). Photographs of the experiment are given in Figures 4 and 5. Nozzle throat gap was 0.1397 mm and channel width was 21.93 mm. Due to the difficulty in manufacturing a two-dimensional nozzle, only one was made. Thus, only one throat gap and hence one nozzle exit Mach number was available for these experiments. As will be shown later, this did not limit the experimental results obtained. Mach number was determined from pressure measurements to be about 4.2 at the nozzle exit and 5.9 on the channel mid-plane. The side planes of the channel were made of borosilicate crown glass to facilitate flow visualization. A standard schlieren optical system was used to photograph the flow. Two different length channels were used--one 80 mm long and the other 37 mm long.

The vacuum system consisted of a 5 x 10^3 liter vacuum tank, a 1500 ℓ/m roughing pump, and a liquid nitrogen cold trap. Vacuum pressures were measured with a Baratron and a thermocouple vacuum gage.

Supersonic nozzle flow was regulated with a high pressure, high flow rate pressure regulator, capable of maintaining stagnation pressure in the nozzle plenums to within about 2 percent. Secondary flow was injected into the main supersonic flow with a two-dimensional nozzle (0.4 mm x 19 mm exit orifice). Combustible gases entered the nozzle separately and mixed as they flowed through it. Mass flow rates were measured with a Thermo Systems series 1352 mass flow transducer. Either liquid nitrogen or water was used to cool the secondary flow nozzle.

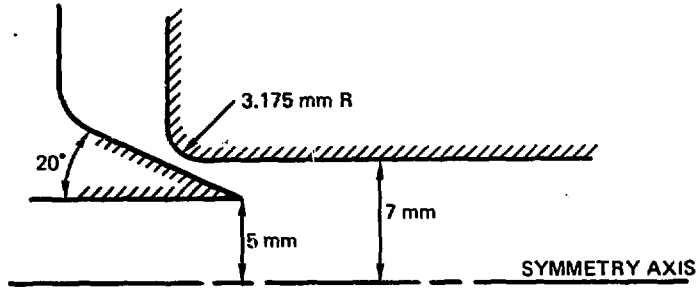

Figure 3. Geometry of Two-Dimensional Nozzle

Figure 4. Experimental Setup

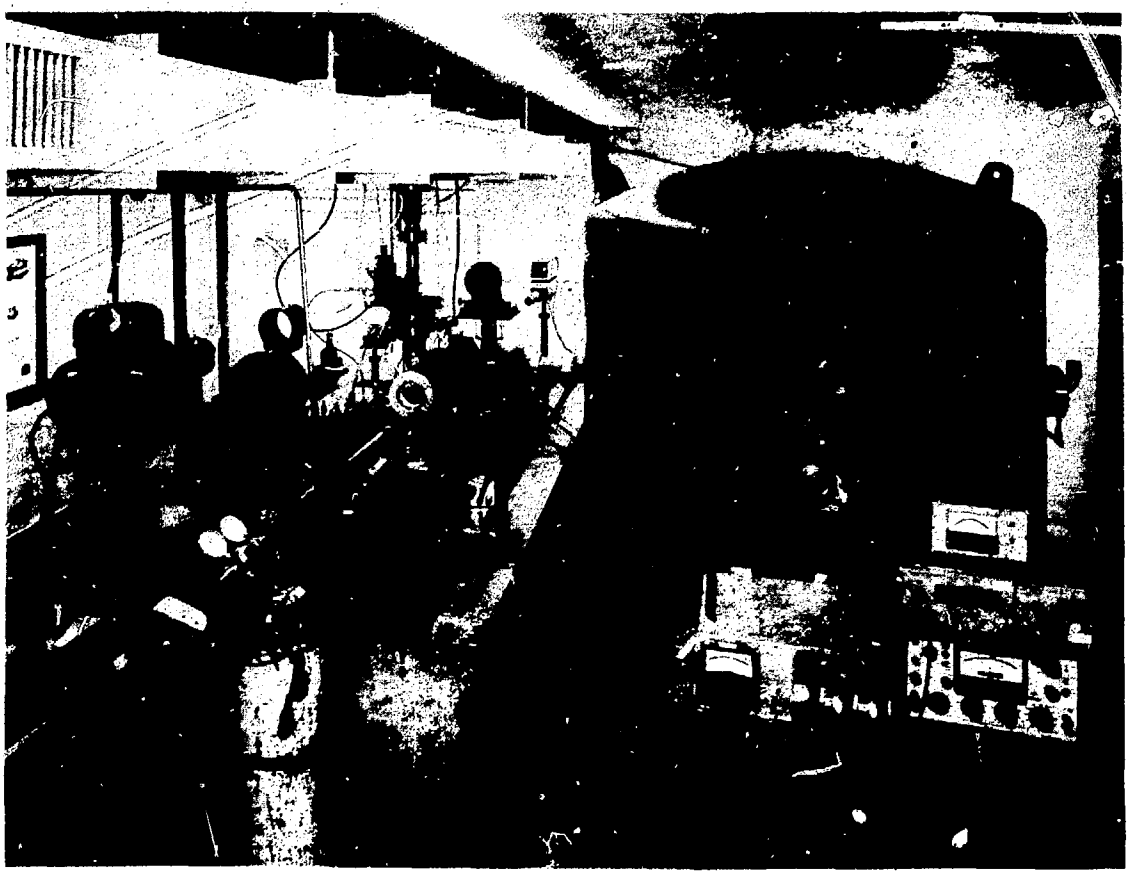

Figure 5. Experimental Setup

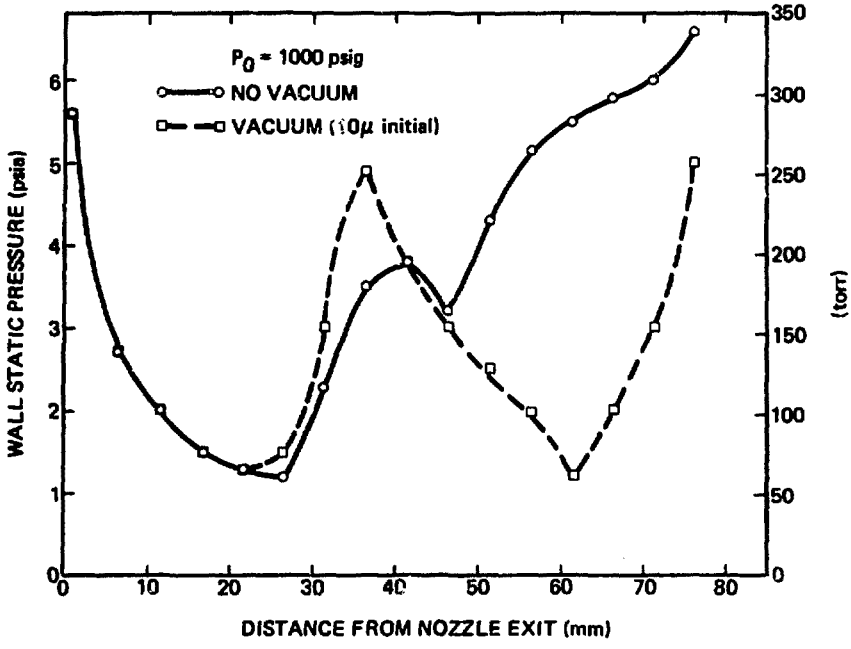

Figure 6. Wall Static Pressure Distribution (80 mm channel)

RESULTS AND DISCUSSION

Wall Pressure Measurements

In Figure 6, wall static pressure distributions both with and without vacuum applied to the vacuum port (see Figure 2) are shown. These pressures are compared to schlieren photographs of the flow in Figure 7 (no vacuum) and Figure 8 (vacuum applied). Pressures were measured along the lower channel wall in both of these pictures. For both cases static pressures decrease downstream of the nozzle exit since the supersonic flow continues to expand into the channel. This expansion can be idealized as taking place from a two-dimensional, inviscid supersonic source (Figure 9). Here streamlines emanating from the source have constant properties along an arc of length $r\theta_0$. The expansion proceeds until streamline OA is turned by the symmetrical jet flow (replaced here by a solid boundary, since the flow is assumed to be inviscid). Streamline OA is turned through an angle θ_0 and a planar, oblique shock wave AC is generated. This shock wave is generated as though a uniform supersonic flow turns through angle θ_0 at the Mach number of streamline OA. Streamlines along arc AB undergo a further isentropic expansion between AB and AC, just as though they were still expanding from the supersonic source. Thus, streamlines enter the shock wave with a Mach number that increases along AC and with entrance angles which decrease along AC. Behind the shock a non-parallel flow results and each streamline has a different entropy, giving rise to a slightly rotational flow field.

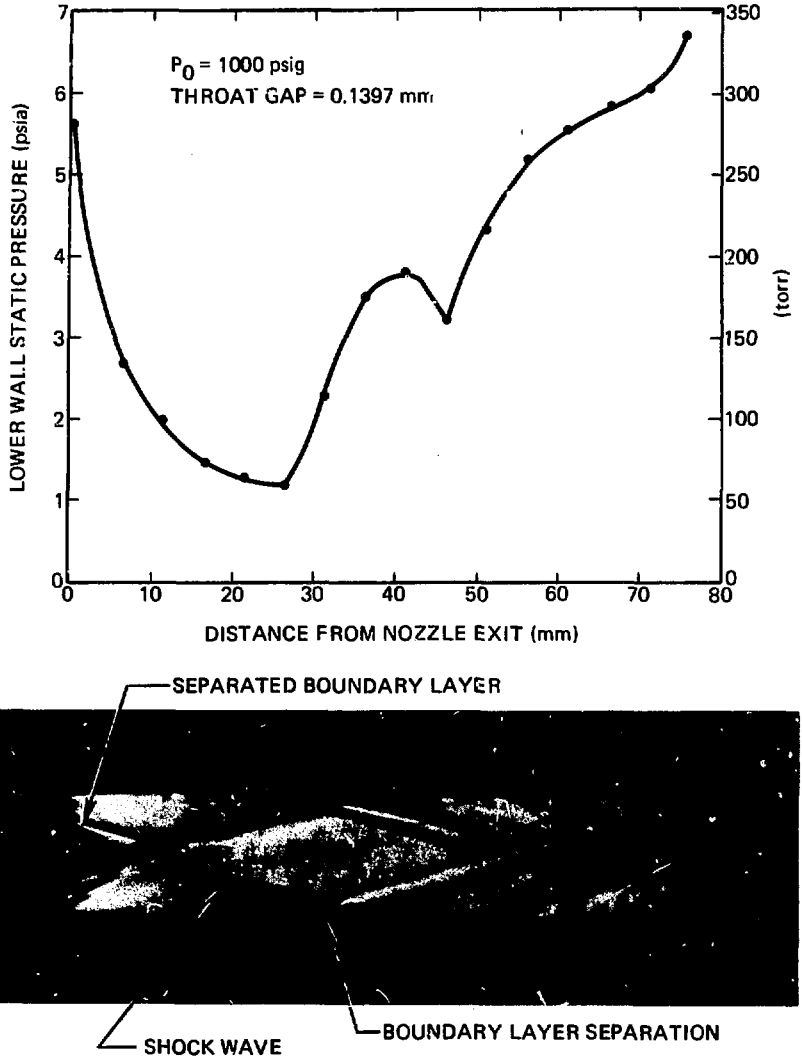

Figure 7. Schlieren photograph and wall pressure distribution for 80 mm long channel; no vacuum applied at left boundary. P_0 is the nozzle stagnation pressure.

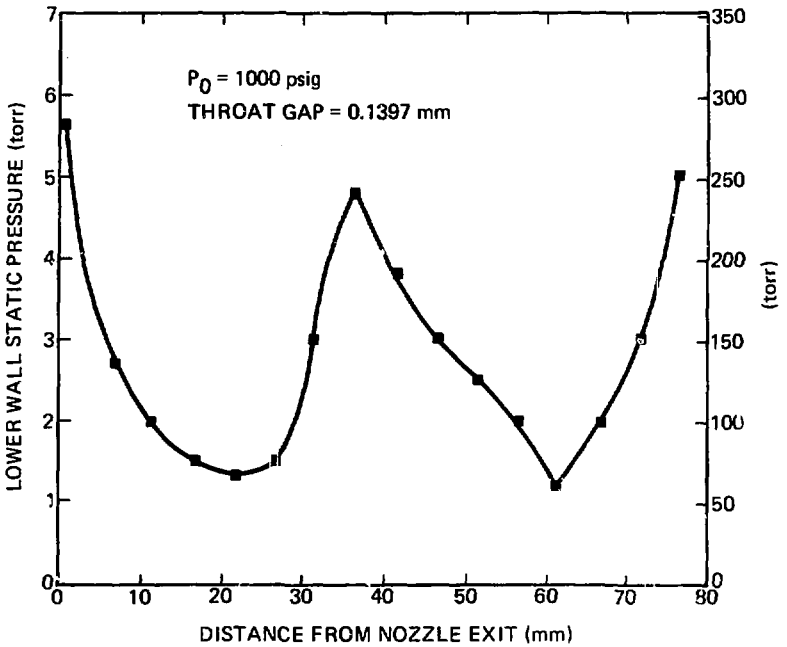

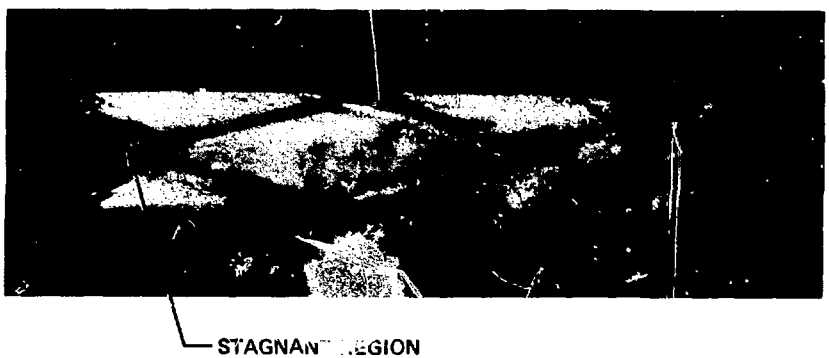

Figure 8. Schlieren photograph and wall pressure distribution for 80 mm channel; vacuum applied at left boundary. P_0 is the nozzle stagnation pressure.

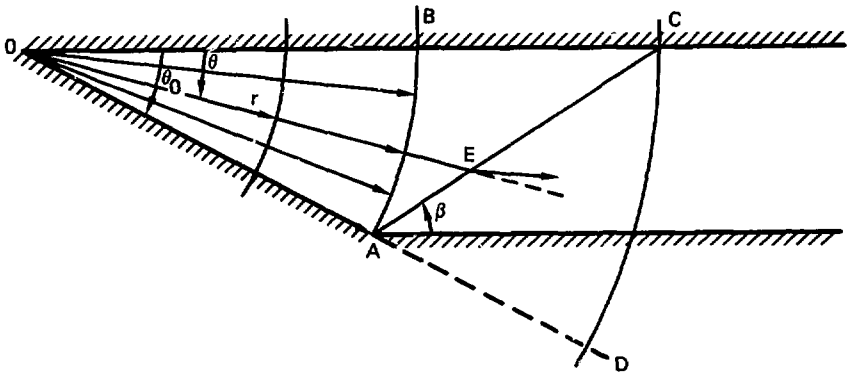

Figure 9. Supersonic source flow. Turning through angle θ_0 causes planar shock AB at angle β.

Using the experimentally obtained angle θ_0 as input, one can calculate several flow field parameters using the above model. The predicted shock wave angle is almost exactly the experimental value. Predicted wall pressure distribution is less than experimental values because of boundary layer effects, which were omitted from the analysis. However, predicted wall pressures before and after shock impingement bracket the measured values. For the INS asymmetric geometry it is believed that the fluid physics remain qualitatively the same (i.e., a straight shock emanates from the flow collision point on the centerline) but is complicated somewhat by the conical flow field in that geometry.

In the schlieren photograph of Figure 7, the first bright-dark line which appears to emanate from the nozzle is the separated nozzle boundary layer, which is visible due to the strong thermal (and thus density) gradient through the boundary layer. Gas near the nozzle wall is at approximately the wall temperature (room temperature initially) while the gas outside the boundary layer is below 100 K. Although this is below the critical temperature, liquification of nitrogen did not occur because insufficient residence time at this temperature did not allow for the growth of nucleation sites. No distinct region is visible along the outside walls because the boundary layer remains attached to those walls while it must separate from the inside walls simply because they end at the nozzle exit plane. The effects of applying suction to this separated flow are shown in Figure 8. Suction appears to thicken the dark region, with the brightness diminishing as the vacuum port is approached. The interpretation of this is that suction "peels off" part of the low energy part of the boundary layer and accelerates some of it into the vacuum port. This acceleration causes a density gradient which in turn causes the change in tone in the photographs. Pressure measurements in this region support this premise (see later section).

The planar shock wave resulting from flow impingement and turning is clearly visible in Figures 7 and 8. Suction appears to change the shock-wall boundary layer impingement point (i.e., about 27 mm in Figure 7 and about 22 mm in Figure 8). The mechanism causing the reflected oblique shocks is described in Shapiro.[1] Simply stated, the incident oblique shock causes the boundary layer to separate, which gives rise to compression waves which in turn coalesce to form the first reflected shock. The second reflected shock comes from refraction of the initial shock wave in the boundary layer. Channel wall boundary layer separation and reattachment is evident in both photographs. The decrease in wall static pressure at about 40 mm in Figure 7 is believed to be attributed to the flow expansion which accompanies boundary layer reattachment. The decrease in static pressure between 36 and 60 mm in Figure 8 seems to extend over too great a distance to be caused by boundary layer reattachment and is not fully understood.

The glass windows were replaced with simulated windows constructed of metal with static pressure taps drilled in them along the mid-plane for the measurements shown in Figure 10. Since the flow static pressure is impressed through the boundary layer over these metal windows and since the two-dimensional flow is approximately constant in a plane perpendicular to the metal windows, these measured static pressures are close to the static pressures that would be measured by a mid-plane static pressure probe. The stagnation point (highest static pressure) appears to be at about 10 mm, which is in approximate agreement with the photographs in Figures 7 and 8.

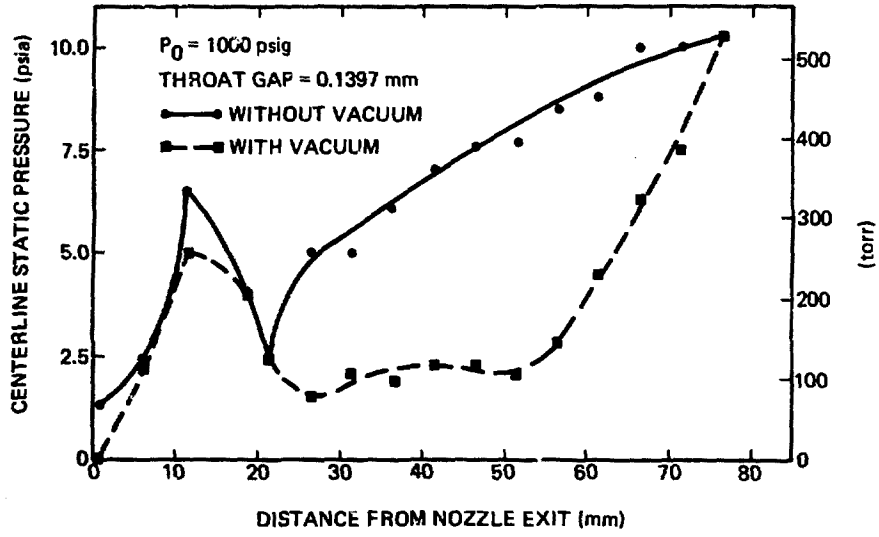

Figure 10. Centerline Static Pressure

Cold Flow Leakage Rates

Leakage flow rates into the vacuum channel were obtained by opening the vacuum tank to the channel flow and allowing the subsequent leakage flow to fill the vacuum tank for a short time period. After thermal equilibrium, measurement of the pressure rise in the vacuum tank was used to determine the mass of gas transferred to the tank. With the measured time of filling, leakage flow rate was determined.

A transient energy and mass balance on the vacuum tank showed that the pressure rise ΔP in the tank is linear with fill time t. This means that the slope of the ΔP,t curve is constant for a fixed nozzle mass flow rate and thus $d(\Delta m)/dt \propto d(\Delta P)/dt$ = constant, where Δm is the change in mass in the tank. Thus, precise control over the vacuum tank fill time between experiments was not required. Typical initial vacuum tank pressures P_V were 10 microns and final pressures were 500 microns.

Measured values of nitrogen leakage flow are shown in Figure 11. Since the purpose of the two-dimensional experiment was to simulate the axisymmetric INS experiment, it is useful to be able to estimate the axisymmetric hydrogen results of Figure 11 using the two-dimensional nitrogen results. To do this, two corrections to the two-dimensional data are necessary. These will be discussed below.

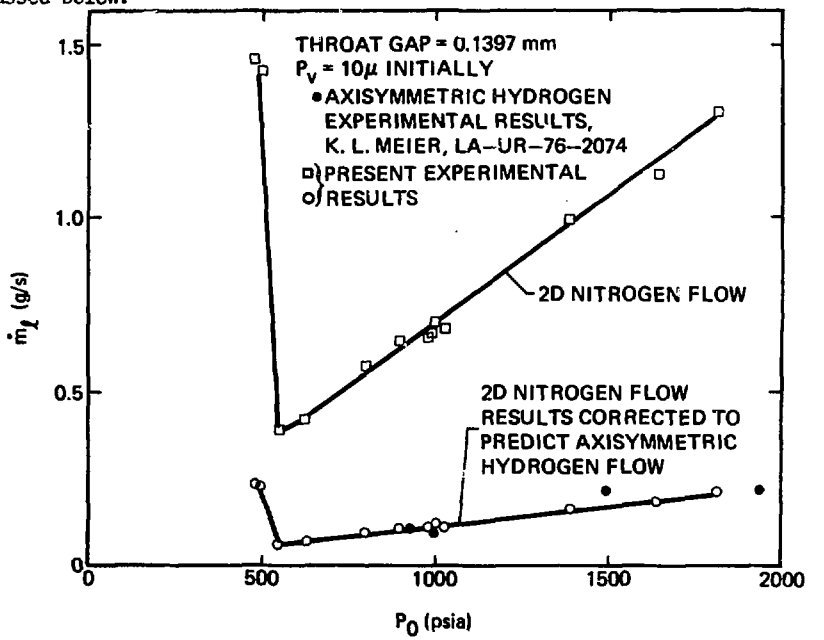

Figure 11. Two-dimensional nitrogen leakage flow rate and comparison of estimated axisymmetric and measured hydrogen leakage flow rate.

It is assumed that the major part of the leakage flow arises from the inability of part of the low energy boundary layer to overcome the pressure gradient imposed on it by the low pressure in the vacuum port and the relatively high pressure in the flow interaction region. For two supersonic nozzles (with the same stagnation conditions and the same ratio of specific heats) identical in cross section except that one is axisymmetric and the other two-dimensional, the Reynolds number ratio at the nozzle exit can be written

$$Re_1/Re_2 = (\hat{M}_1/\hat{M}_2)^{1/2} (\mu_2/\mu_1)(A_e/A^*)_2/(A_e/A^*)_1$$

where 1 denotes the two-dimensional nozzle with nitrogen and 2 represents an axisymmetric nozzle with hydrogen. $\hat{M}$, μ, A_e, and A^* represent molecular weight, viscosity, exit area, and throat area, respectively. For the two-dimensional nozzle, the corresponding areas are $A_e = L(y_0-y_e)$, $A^* = L(y_0-y_i)$, and $(A_e/A^*)_1 = (y_0-y_e)/(y_0-y_i)$, where L = channel width, y_0-y_i is the throat gap, and y_0-y_e is the exit gap.

For the axisymmetric nozzle, $A_e = \pi(r_0^2-r_e^2)$, $A^* = \pi(r_0^2-r_i^2)$, and $(A_e/A^*)_2 = (r_0^2-r_e^2)/(r_0^2-r_i^2)$, where r_0, r_e, and r_i are the radii of the outer channel wall, nozzle exit, and nozzle throat, respectively.

For a two-dimensional and axisymmetric nozzle having $r_0 = y_0 = 7$ mm, $r_0-r_i = y_0-y_i = 0.1524$ mm, and $r_e = y_e = 5$ mm,

$$(A_e/A_e^*)_2/(A_e/A_e^*)_1 = 0.8677 \quad ,$$

the difference from unity is attributable to the differences between the two-dimensional and axisymmetric geometries.

Substituting values into the previous Reynolds number expression yields $Re_1/Re_2 = 1.67$. For practical engineering purposes, the Reynolds numbers are the same at the nozzle exits and one can expect the boundary layers to have approximately the same properties there. Now the corrections to the two-dimensional data can be made.

The first correction is based on the argument that for the same Reynolds number at the nozzle exit, a simple linear correction based on the perimeter over which the boundary layer exists at the nozzle exit should account for differences in flow geometries. The boundary layer perimeter in the axisymmetric geometry is $P_{as} = 2\pi r_e$, while in the two-dimensional geometry $P_{2d} = 2L + 4\ell$ where ℓ is the wetted side length at the nozzle exit (Figure 12). For the geometries involved, $P_{as}/P_{2d} = 0.606$.

The second correction accounts for the differences between nitrogen and hydrogen as main flow gases. The flow in the ion beam port must be at least choked, since the pressure ratio is essentially infinite and the duct area is constant. The choked flow relationship is

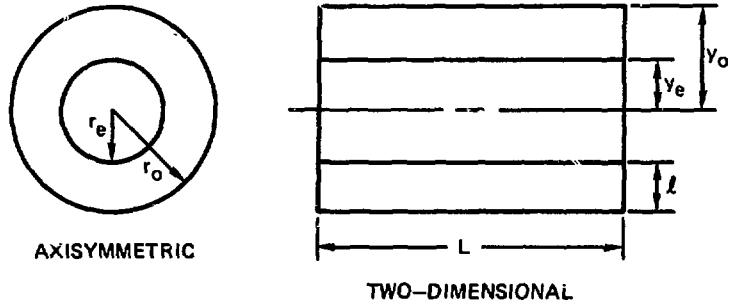

Figure 12. Parameters used in boundary layer calculations.

$$\dot{m}_\ell \propto A^* \left[\frac{\gamma}{R} \left(\frac{2}{\gamma + 1} \right)^{\frac{\gamma + 1}{\gamma - 1}} \right]^{1/2} \frac{P_0}{\sqrt{T_0}}$$

where $\dot{m}_\ell$ is the leakage mass flow rate and the proportionality sign is used to account for loss of plenum stagnation pressure through viscous action in the boundary layer. γ, R, P_0, and T_0 are specific heat ratio, gas constant per unit mass, stagnation pressure, and stagnation temperature, respectively.

We arrive at the following ratio:

$$\frac{\dot{m}_{\ell_{N_2}}}{\dot{m}_{\ell_{H_2}}} = \left(\frac{\hat{M}_{N_2}}{\hat{M}_{H_2}} \right)^{1/2} = 3.74$$

The leakage flow data obtained on the two-dimensional experiment (throat gap 0.1397 mm) using nitrogen was corrected using the above arguments (each data point was multiplied by the factor 0.606/3.74) and compared to data obtained at LASL on a nearly identical axisymmetric experiment (throat gap 0.1524 mm) using hydrogen. Excellent agreement resulted, as seen in Figure 11.

When the nitrogen leakage flow is nondimensionalized by the nozzle mass flow rate $\dot{m}_1$, the plot in Figure 13 results. The ratio $\dot{m}_\ell/\dot{m}_1$ is not a function of nozzle stagnation pressure P_0 once the system "starts" because $\dot{m}_\ell$ must be proportional to P_0, as was assumed above.

Figure 14 is leakage flow data obtained at LASL (Reference 2) for different nozzle throat spacings. The solid lines are the author's best fit approximations to the data. It would be useful if all of this data could be collapsed onto a single curve. This can be approximately accomplished as follows.

The mass flow rate through the axisymmetric nozzle is

$$\dot{m} = A^* \left[\frac{\gamma}{R} \left(\frac{2}{\gamma + 1} \right)^{\frac{\gamma + 1}{\gamma - 1}} \right]^{1/2} \frac{P_0}{\sqrt{T_0}}$$

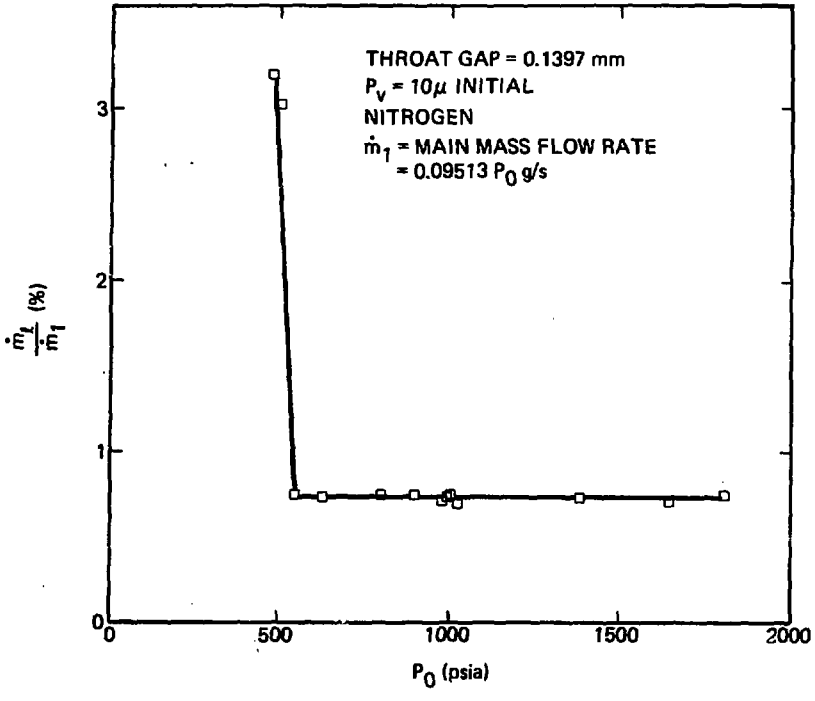

Figure 13. Dimensionless Leakage Flows

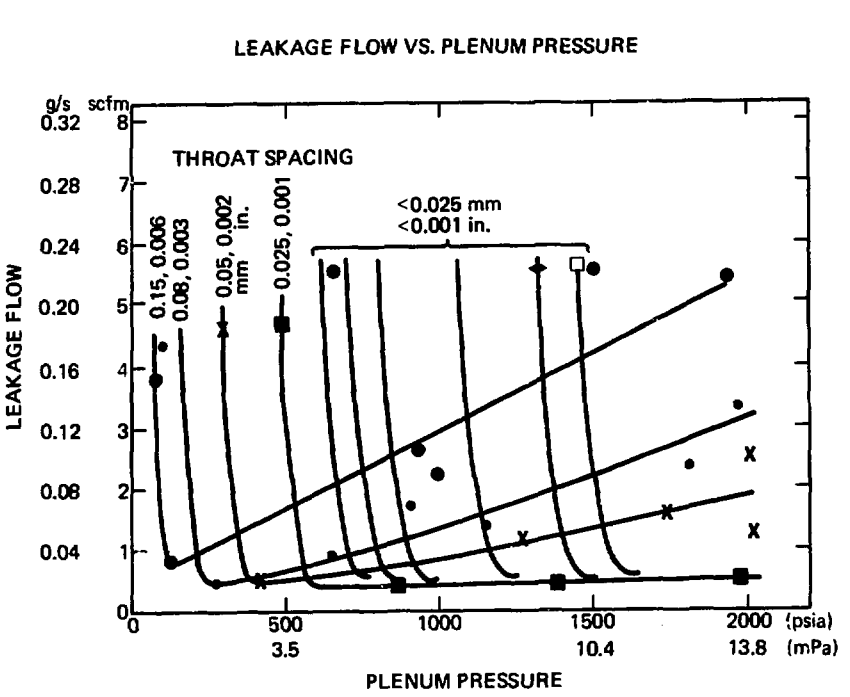

Figure 14. Leakage flow measurements made at LASL by K. L. Meier (LA-UR-76-3074).

A ratio of nozzle mass flows for two experiments identical in every detail except the throat spacing is

$$\dot{m}_1/\dot{m}_2 = A_1^*/A_2^*$$

since the other parameters cancel out. As the nozzle throat area decreases, the mass flow rate diminishes for the same stagnation conditions. This reduced mass flow rate decreases the mass flow rate in the boundary layer, part of which is assumed to spill into the ion beam port. Thus, the leakage mass flow must be diminished in the same manner in which the nozzle mass flow is diminished.

The above ratio of mass flow rates can be written (for an axisymmetric geometry)

$$\dot{m}_1/\dot{m}_2 = (r_0^2-r_i^2)_1/(r_0^2-r_i^2)_2 \quad ,$$

This ratio can be factored to yield

$$\dot{m}_1/\dot{m}_2 = \frac{(r_0-r_i)_1}{(r_0-r_i)_2}\frac{(r_0+r_i)_1}{(r_0+r_i)_2} = \frac{\Delta r_1}{\Delta r_2}\frac{(r_0+r_i)_1}{(r_0+r_i)_2}$$

For small throat gaps, $r_0 \simeq r_i$, so that

$$(r_0+r_i)_1/(r_0+r_i)_2 \simeq 1$$

However, the ratio $\Delta r_1/\Delta r_2$ can be large.

Thus, a simple linear correlation based on throat gap must exist; i.e.,

$$\dot{m}_1/\dot{m}_2 \approx \Delta r_1/\Delta r_2$$

Define a dimensionless leakage mass flow parameter to be

$$\frac{\dot{m}}{\dot{m}^*}\frac{\Delta r^*}{\Delta r}$$

where $\dot{m}^*$ is the leakage flow for a reference throat spacing of 0.1524 mm (large circles shown in Figure 14), Δr^* is that reference throat spacing, $\dot{m}$ is the leakage mass flow rate, and Δr is throat spacing.

If the fitted results shown in Figure 14 are plotted with this new dimensionless parameter as the ordinate, Figure 15 results. Note that all the data (spanning about an order of magnitude in throat spacing) lie on a single curve, except for the high pressure, small throat gap spacing results. This deviation may represent some nonlinear boundary layer effect. As can be seen in Figure 14, different starting pressures exist for different throat spacings. However, the starting pressures are approximately given by $P_0^* \Delta r^*/\Delta r$, where P_0^* is the starting pressure for the reference data curve.

The above described correlation collapses nearly all of the data of Figure 14 onto the single dimensionless leakage curve of Figure 15. This curve, however, is the very one that can be estimated from the two-dimensional nitrogen leakage results shown in Figure 11. Thus, with a single throat spacing in the two-dimensional geometry using nitrogen as the main flow gas, it is possible to estimate the axisymmetric leakage flow rates over a wide range of throat spacings using hydrogen as the main flow gas.

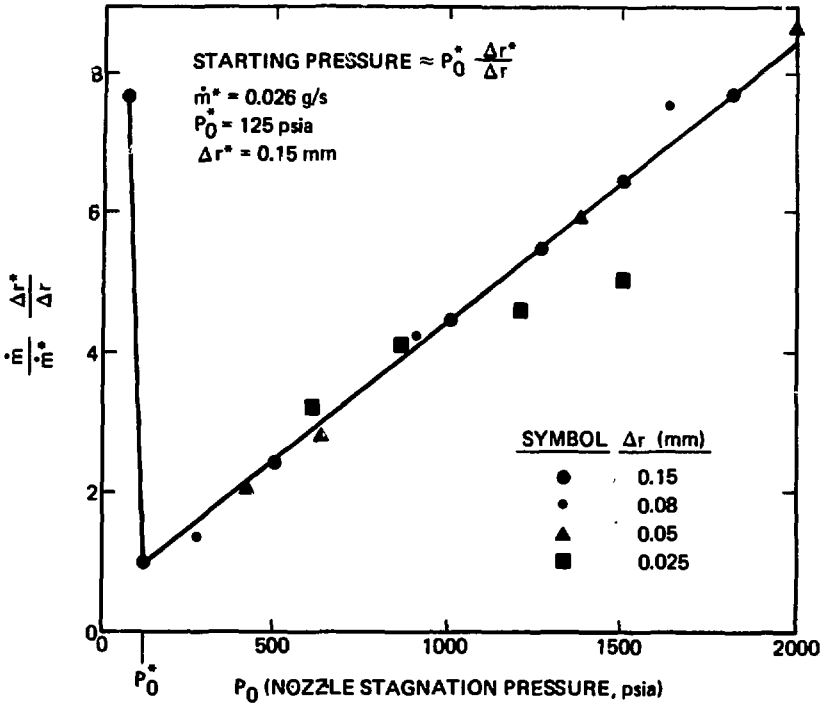

Figure 15. Dimensionless Leakage Flow Curve

Vacuum Channel Pressure and Mach Number

Vacuum channel centerline pitot pressure measurements are shown in Figure 16. The plateau in pitot pressure results from a stagnant-subsonic region in the flow. Recall that pitot pressure remains constant in either a stagnant or subsonic region due to the absence of a normal shock wave in front of the probe. Pitot pressure decreases to the right of this plateau because the main flow aspirates the probe. A photograph of the pitot probe at the point of aspiration is shown in Figure 17. Pitot pressure diminishes to the left of the plateau because the flow has become supersonic (a normal shock wave in front of the flow accounts for the total pressure loss). Of interest is that a supersonic flow begins in space prior to the flow entering the two-dimensional vacuum channel. While inside the vacuum channel, the flow appears to increase slightly in Mach number (as evidenced by the decrease in pitot pressure which would result as the flow Mach number increases giving a larger total pressure loss through the normal shock). At the exit of the two-dimensional channel the flow appears to shock-down and become subsonic (constant pitot pressure), after it enters the large axisymmetric portion of the vacuum channel. Scatter in the data inside the vacuum channel is due to the inability to accurately center the probe in what must be a two-dimensional flow field with non-uniform Mach number.

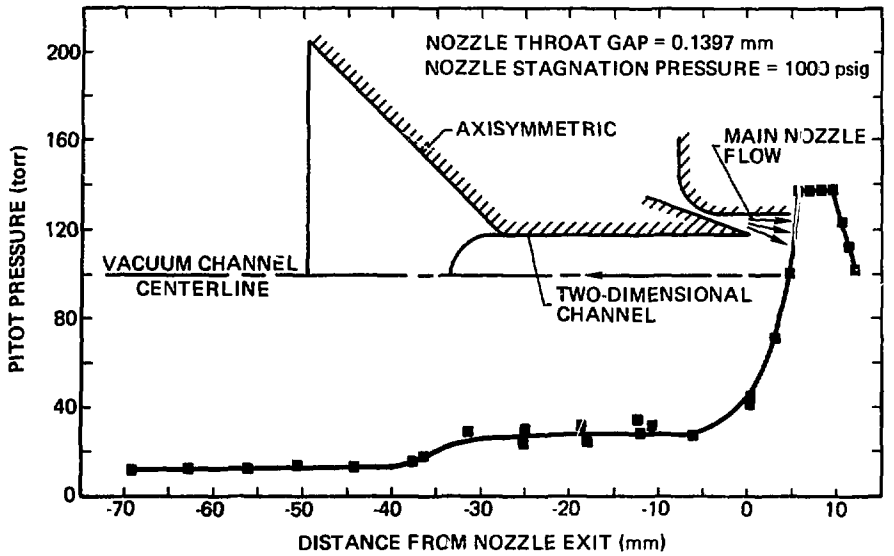

Figure 16. Vacuum Channel Centerline Pitot Pressure

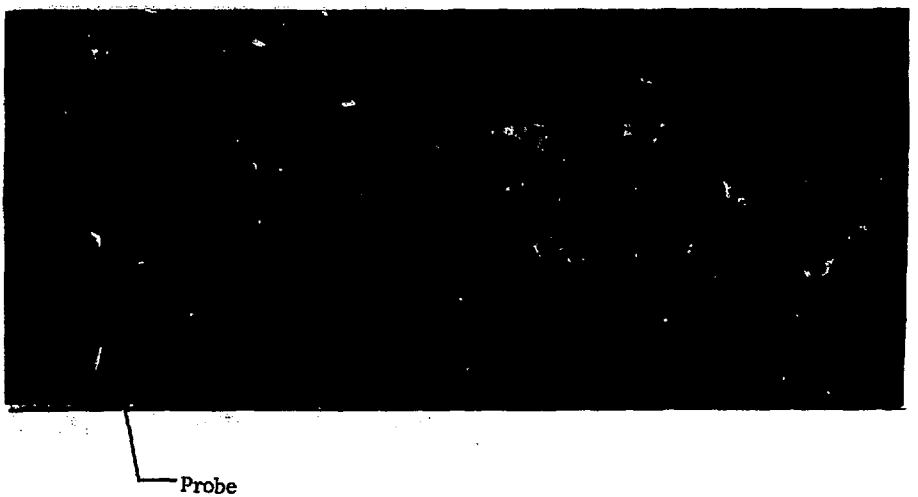

Figure 17. Pitot Probe at Downstream Point of Aspiration

Calculated centerline Mach number is given in Figure 18. In making this calculation it was assumed that the flow stagnation pressure remained at its level in the plateau region. This, along with the subsequent measured pitot pressure, gave all the information needed to calculate Mach number. With this procedure it is not possible to calculate the flow Mach number once the flow becomes subsonic, since the strength of the shock wave which causes the flow to become subsonic is not known. All that can be said is that the flow is "most probably" subsonic after this point. However, the plateau Mach number (M) (subsonic) was calculated with knowledge of the static pressure in the plateau region.

The flow in this experiment is somewhat unusual since there is hypersonic flow (M > 5) to the right of the stagnant region and supersonic flow (M ≈ 3.5) to the left of this region. Similar flow would result for hypersonic flow over the aft portion of a body having base suction.

Leakage Flow Rates with Mass Addition to and Momentum Extraction from the Main Flow

The equivalence between mass, momentum, and energy addition to a compressible flow is well known. In Reference 3 a similarity parameter $\lambda = (1+c)(1+a)/(1+b)^2$ based on a one-dimensional analysis was derived where a,

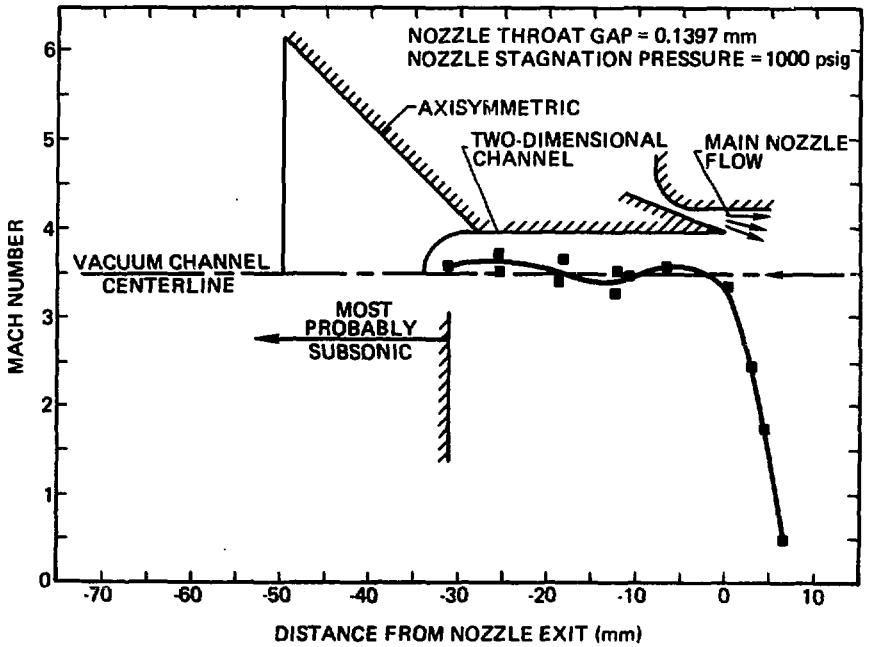

Figure 18. Calculated Centerline Mach Number

b, c are dimensionless mass, momentum, and energy addition. Two flows having different levels of mass, momentum, and energy addition can be made similar in terms of reduced flow quantities (see Reference 3) if the value of λ between the two flows is the same.

Cold flow leakage measurements were performed in which equivalent energy was added to the supersonic channel flow by mass addition and momentum extraction. Figure 19 shows the data obtained from that experiment for a single main flow stagnation pressure. The presence of the secondary flow nozzle (with zero mass flow through it) does not affect the leakage flow. However, there is an unexplained jump in leakage flow with the initiation of secondary flow addition. Leakage flow level remains constant in what the author calls the weak shock regime (discussed later) until transition to the strong shock regime. This transition is accompanied by about a 20 percent increase in leakage flow.

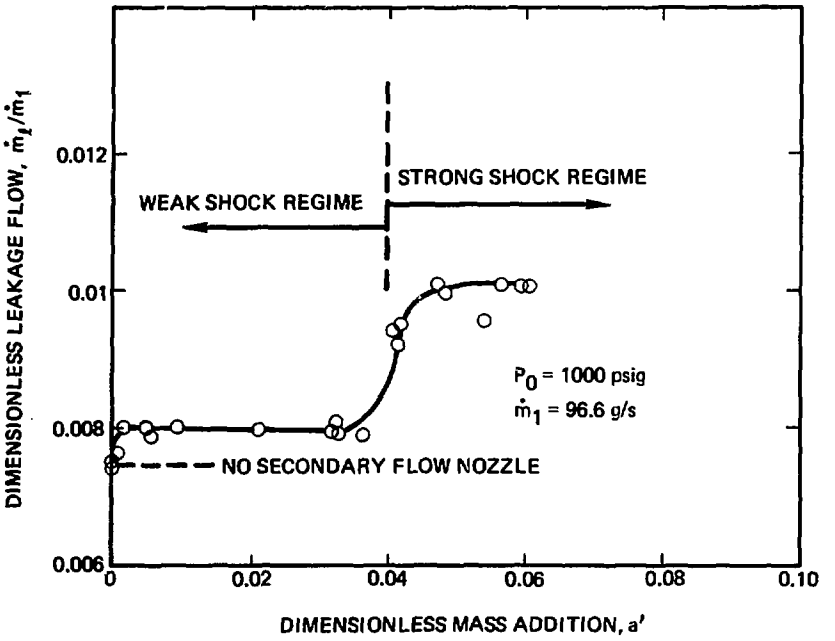

Figure 19. Leakage flow versus mass addition. $a' = \dot{m}_s/\dot{m}_1$, where $\dot{m}_s$ is the secondary mass flow rate and $\dot{m}_1$ is the primary mass flow rate.

Equivalent INS energy deposition is estimated from

$$c = \frac{(1 + a')^2}{(1 - a'\tilde{G})^2} - 1$$

where a' is dimensionless mass addition in the two-dimensional nitrogen experiment and $\tilde{G}$ is the momentum dissipation function defined in Reference 3. Leakage flow as a function of equivalent INS energy deposition divided by the maximum INS energy deposition (downstream Mach number of unity), is given in Figure 20. Note that with mass addition and momentum extraction, it was possible to achieve only about 30 percent of the theoretical maximum INS energy deposition level. Also given in Figure 20 is the two-dimensional nitrogen data corrected to estimate axisymmetric hydrogen leakage flow rates. The correction was the same one used in Figure 12.

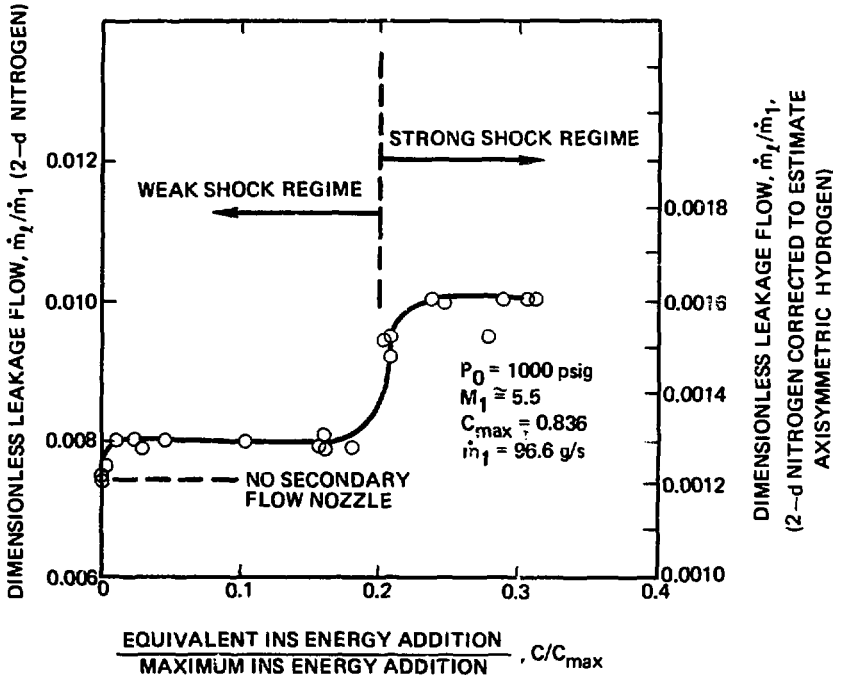

Figure 20. Leakage Flow Versus Equivalent Energy Addition

A schlieren photograph of the channel flow with zero secondary flow and no vacuum is shown in Figure 21 and the same flow with vacuum applied is given in Figure 22. Also given in these figures are the static wall pressures measured along the upper channel wall. Similar results for small secondary mass flow rates (weak shock regime) are given in Figures 23 and 24 and for large secondary mass flow rates (strong shock regime) in Figures 25 and 26. Although the bow shock in front of the secondary flow nozzle is more normal in the strong shock regime than in the weak shock regime, the flow downstream still appears to be supersonic (presence of compression waves in photograph). This observation is consistent with the fact that only 30 percent of the maximum INS energy has been added to the flow. At the maximum level of energy addition, the Mach number downstream of the energy addition region is unity.

Ignition of Secondary Flow Combustible Gases

The opposed H_2-O_2 jet was very difficult to ignite with nitrogen as the main flow gas due to dilution in the critical region (see Reference 4 for a description of critical region). Ignition via a spark source was attempted at various locations in the flow field. The ignition scheme that worked is shown in Figure 27. Here, a hollow, retractable ceramic rod with a conductor down the center was used to provide a spark through the stagnation region of the combustible gas mixture. However, with the flow rate of combustible gases estimated to be required for maximum energy addition (Reference 3), the subsonic region extending from the bow shock to the burner orifice was too small in extent. This meant that nitrogen streamlines, after passing through the shock, had insufficient time to feel the presence of and go around the burner, thus diluting the combustible gas mixture below its lower combustion limit. Ignition was achieved by increasing the mass flow of combustible gas, pushing the shock further away from the burner exit and achieving a combustible mixture.

The initial burner design did not survive the first hot experiment. The project was terminated before a new burner design could be tested. No hot flow leakage data were thus generated. Such data would have extended the curve shown in Figure 20 to $c/c_{max} = 1.0$.

CONCLUSIONS

The two-dimensional leakage flow results obtained herein using nitrogen as the main flow gas can be corrected by the method outlined herein to estimate leakage flow in an axisymmetric experiment using hydrogen as the main flow gas (INS configuration). It appears as though the major part of the leakage flow arises from a stagnation region in front of the vacuum port that is formed by low energy boundary layer flow from the main nozzles. This leakage flow accelerates to a supersonic Mach number prior to entering the vacuum port and remains at an essentially constant Mach number while travelling through it.

For energy deposition levels up to thirty percent of the theoretical maximum, both a weak and strong shock regime for leakage flow have been identified. In the strong shock regime, leakage flows are about twenty percent greater than they are in the weak shock regime. Dramatic changes in the channel flow shock wave patterns accompany these flow regimes.

Ignition of an opposed H_2-O_2 jet in a hypersonic nitrogen flow is possible.

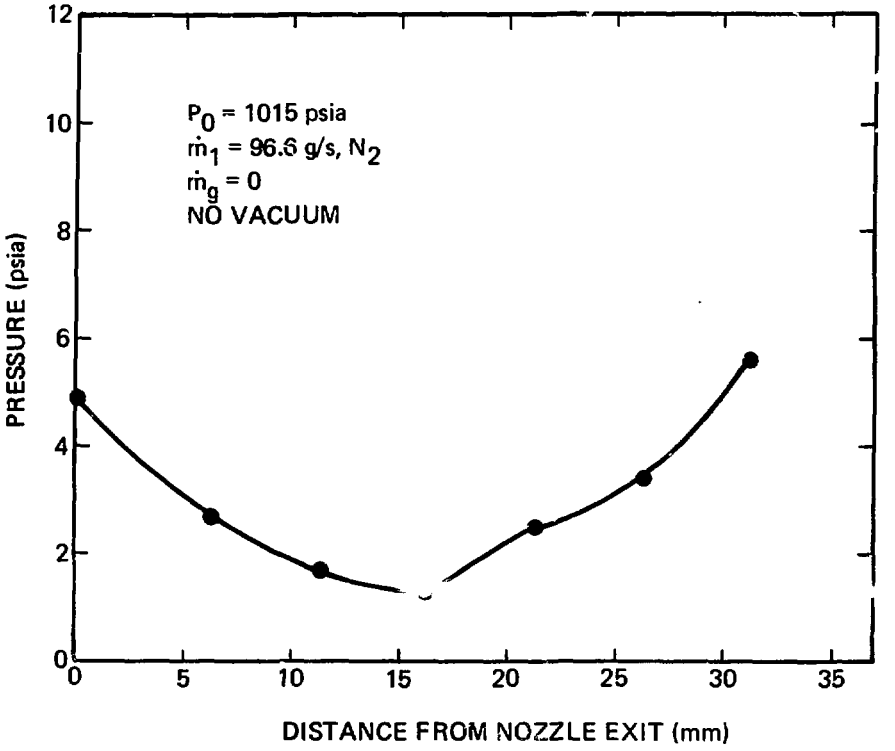

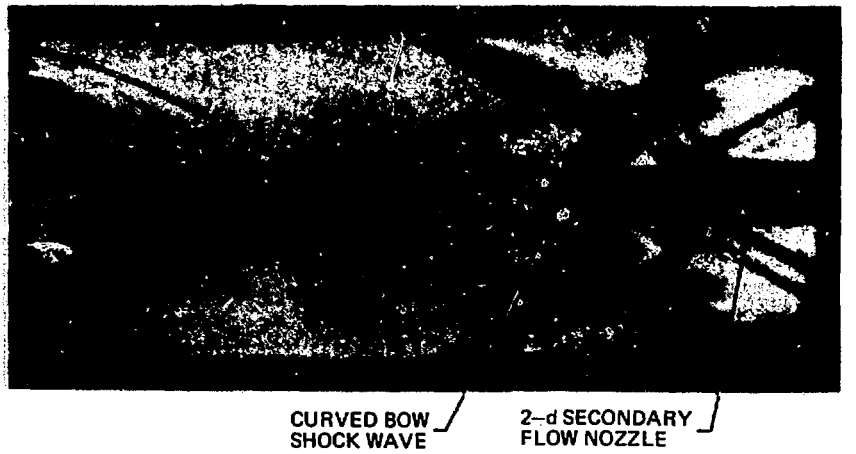

Figure 21. Zero Secondary Flow, No Vacuum

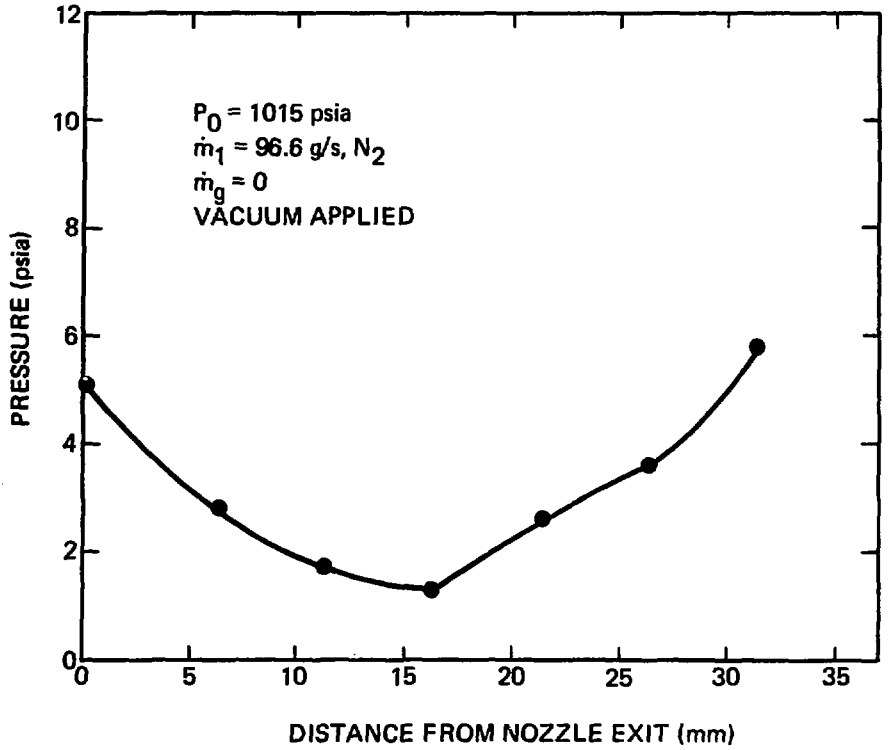

Figure 22. Zero Secondary Flow, Vacuum Applied

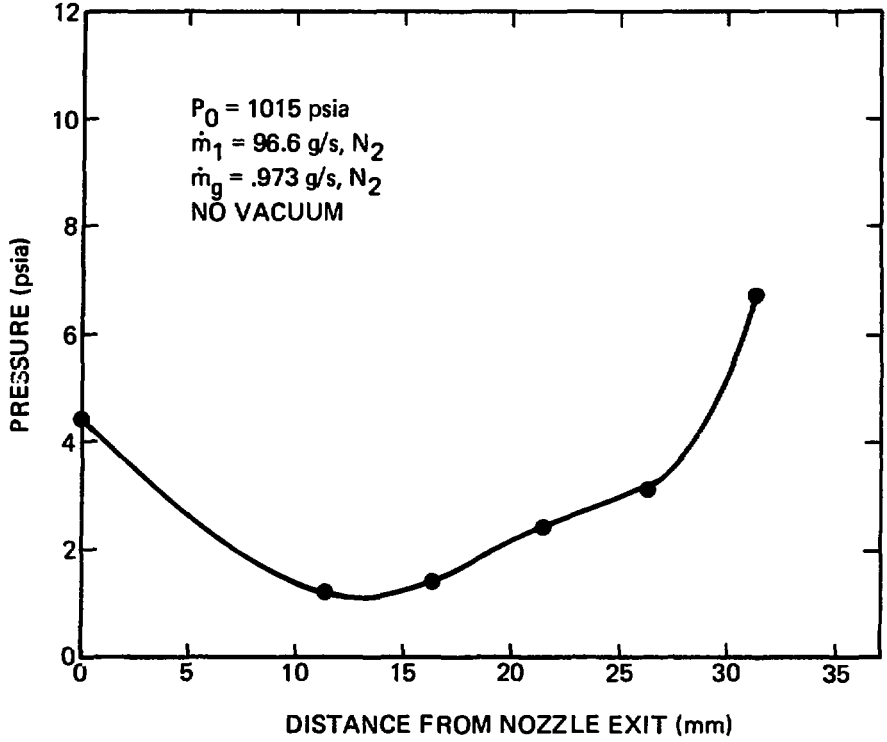

Figure 23. Weak Shock Regime, No Vacuum

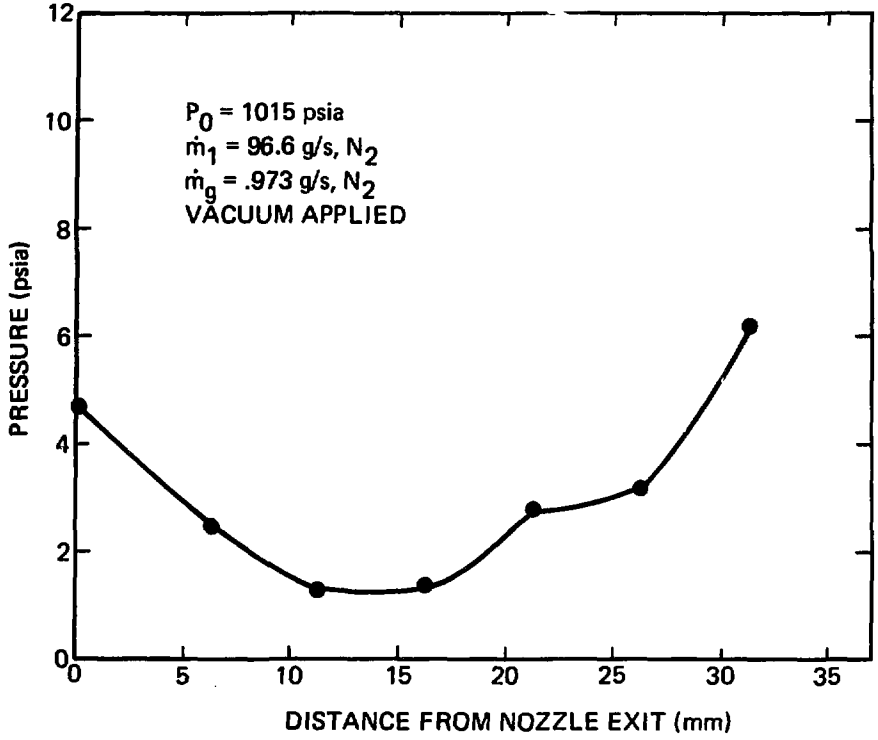

Figure 24. Weak Shock Regime, Vacuum Applied

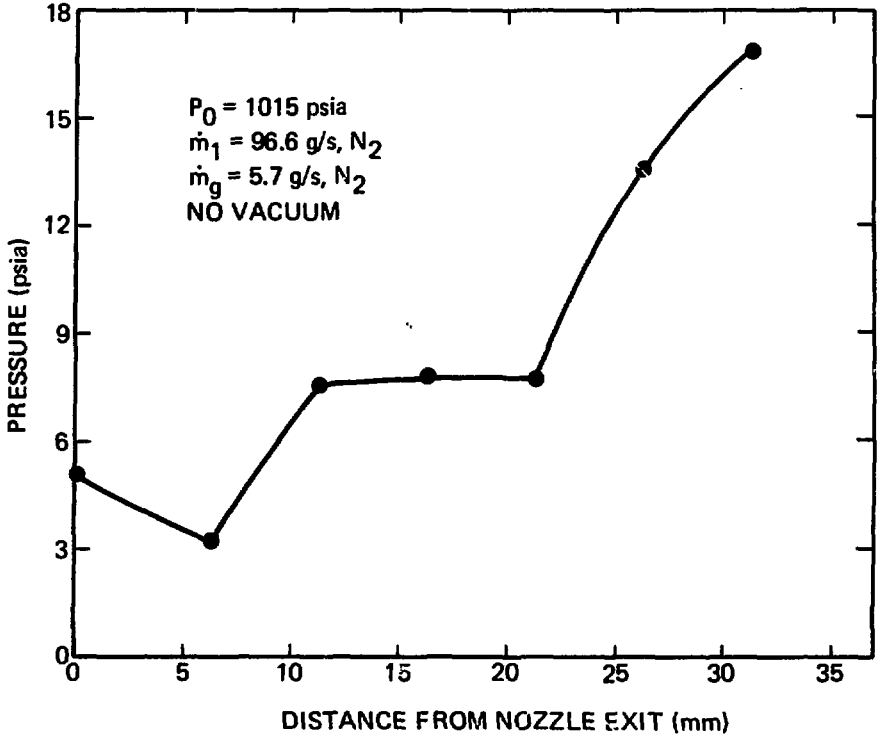

Figure 25. Strong Shock Regime, No Vacuum

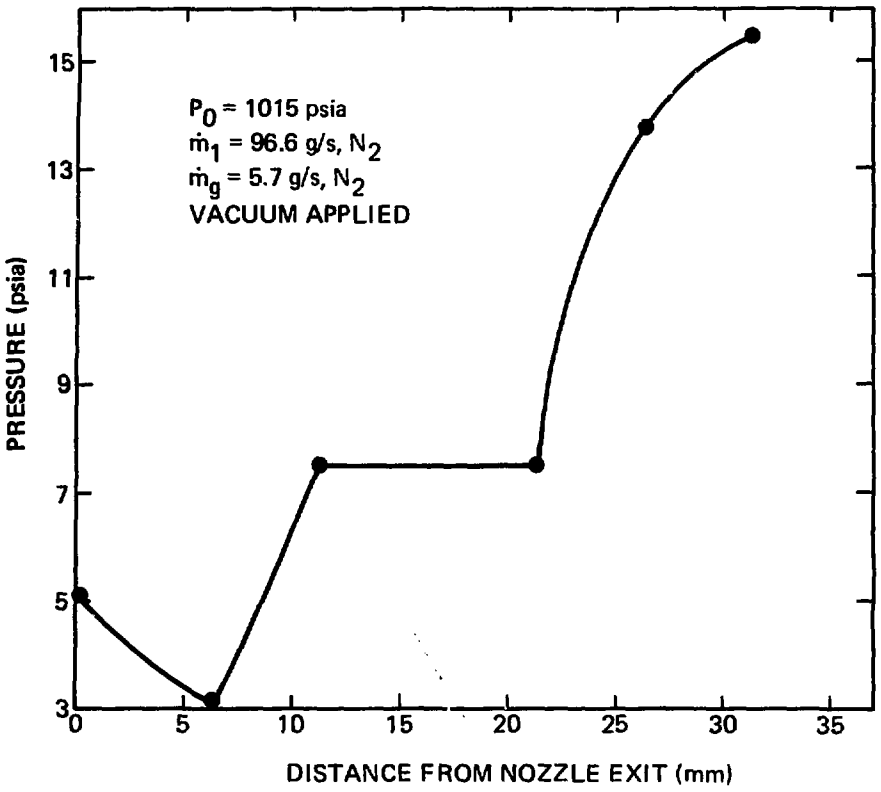

Figure 26. Strong Shock Regime, Vacuum Applied

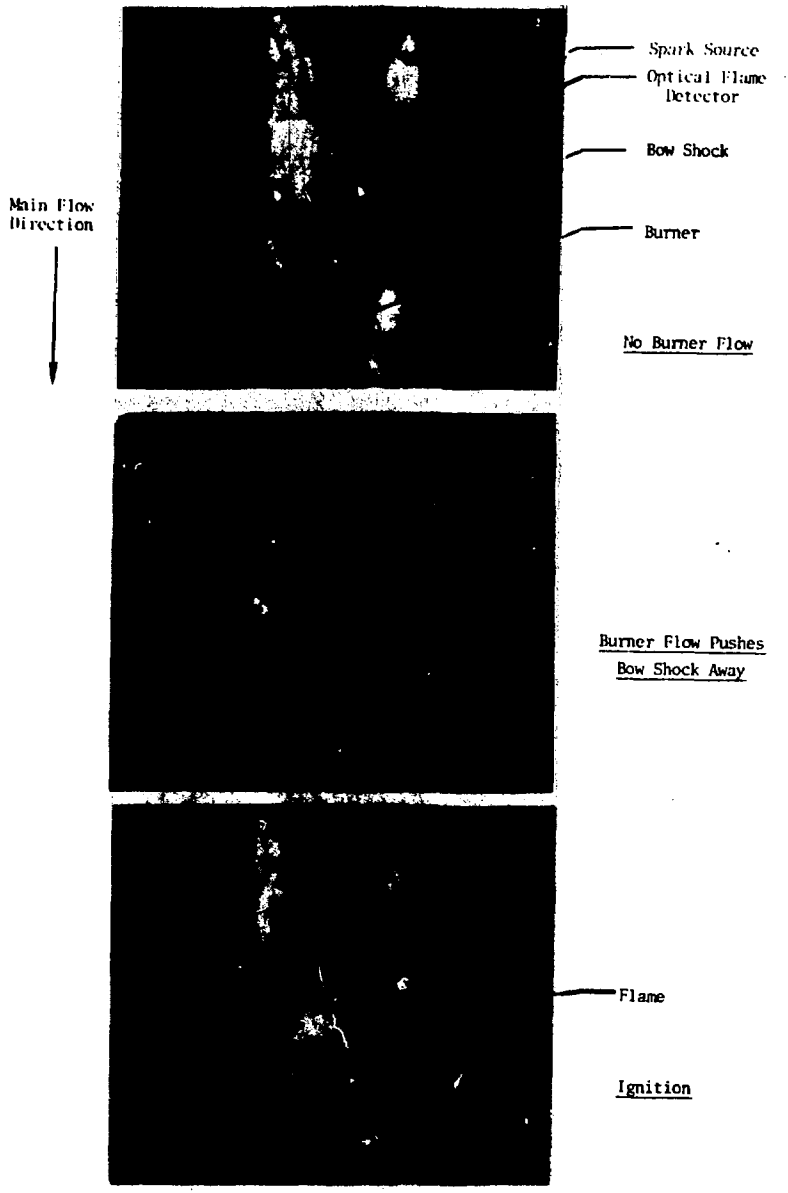

Figure 27. Ignition sequence for combustible gas secondary flow. Photographs are rotated 90° from previous photographs.

REFERENCES

1. A. H. Shapiro, The Dynamics and Thermodynamics of Compressible Fluid Flow, Ronald Press, New York, 1953, Vol. 1, pp. 581,582.

2. K. L. Meier, "Jet Experiments for the Intense Neutron Source," LASL LA-UR-76-2074, Sept. 1976.

3. S. C. Johnston, "A One-Dimensional Model of Steady, Compressible Channel Flow with Mass, Momentum, and Energy Addition," SAND76-8244, Sept. 1976.

4. A. Schaffer, "Phenomenological Analysis of the Opposing Jet Flameholder," Ph.D dissertation, Northwestern University, Evanston, Illinois, June, 1957.